

## Temperature-dependent photoluminescence in $\text{La}_{2/3}\text{Ca}_{1/3}\text{MnO}_3$

T. Ding<sup>a</sup>, W.T. Zheng<sup>a,\*</sup>, H.W. Tian<sup>a</sup>, J.F. Zang<sup>a</sup>, Z.D. Zhao<sup>a</sup>, S.S. Yu<sup>a</sup>, X.T. Li<sup>a</sup>,  
F.L. Meng<sup>a</sup>, Y.M. Wang<sup>a</sup>, X.G. Kong<sup>b</sup>

<sup>a</sup>Department of Materials Science and Key Lab of Automobile Materials of MOE, Jilin University, Qianwei Road 10, Changchun 130023, People's Republic of China

<sup>b</sup>Key Lab of Physics on Excited States Process, Changchun Institute of Optics, Fine Mechanics and Physics, Chinese Academy of Science, Changchun 130033, People's Republic of China

Received 27 March 2004; accepted 23 September 2004 by A. Pinczuk

Available online 5 October 2004

### Abstract

Visible photoluminescence and its temperature dependence of  $\text{La}_{2/3}\text{Ca}_{1/3}\text{MnO}_3$  in the temperature range 138–293 K were measured. It was observed that the main broad band centered at  $\sim 1.77$  eV with the shoulders at  $\sim 1.57$  and  $\sim 1.90$  eV existed in the entire temperature range. It can be well fitted by three Gaussian curves  $B_1$ ,  $B_2$  and  $B_3$  centered at  $\sim 1.52$ ,  $\sim 1.75$  and  $\sim 1.92$  eV, respectively. The intensities of the peak  $B_1$  and  $B_2$  vary as temperature increases. In the entire temperature range, the intensity of  $B_1$  increases with increasing temperature, whereas that of  $B_2$  decreases. The photoluminescence mechanisms for  $\text{La}_{2/3}\text{Ca}_{1/3}\text{MnO}_3$  are presented based on the electronic structures formed by the interactions among spin, charge and lattice, in which  $B_1$  was identified with the charge transfer excitation of an electron from the lower Jahn–Teller split  $e_g$  level of a  $\text{Mn}^{3+}$  ion to the  $e_g$  level of an adjacent  $\text{Mn}^{4+}$  ion,  $B_2$  is assigned to the transition between the spin up and spin down  $e_g$  bands separated by Hund's coupling energy  $E_J$  and  $B_3$  is attributed to the transition, determined by the crystal field energy  $E_C$ , between a  $t_{2g}$  core electron of  $\text{Mn}^{3+}$  to the spin up  $e_g$  bands of  $\text{Mn}^{4+}$  by a dipole allowed charge transfer process.

© 2004 Elsevier Ltd. All rights reserved.

PACS: 75.30. – m; 61.20.Lc; 78.55. – m

Keywords: A. Perovskite manganites; B. Photoluminescence; C. Solid state reaction

Perovskite manganites with mixed manganese valence,  $\text{La}_{1-x}\text{A}_x\text{MnO}_3$  with A for a divalent metal, have attracted a great deal of attention due to the anomalously large negative 'colossal' magnetoresistance (CMR) for  $0.2 < x < 0.5$  [1–3]. Understanding the behavior of these Mn-based materials is a challenge for both experimentalists and theorists. It is now accepted that both double exchange (DE) [4] and Jahn–Teller (J–T) lattice distortions [5] play an important role in the magnetic and transport properties of the manganites. Other effects such as magnetic polarons, electron

localization and phase separation of carriers have been advanced as an additional physics [6,7]. These effects show that spin, charge and lattice are strongly coupled in the CMR materials [8]. Although most of the attention has been focused on the effect of applied magnetic field and temperature on the conductivity, there is much to be learned from other properties (such as photoluminescence) determined by the electronic structure in  $\text{La}_{2/3}\text{Ca}_{1/3}\text{MnO}_3$  (LCMO) [8].

Photoluminescence (PL) in solid materials is always resulting from radiative decay of electronic transitions. In semiconductors, the PL comes from band to band transition or excitonic states while in insulators from impurities, as transition metal or rare earth ions. Some few cases that are

\* Corresponding author. Fax: +86 431 5168246.

E-mail address: [wzheng@jlu.edu.cn](mailto:wzheng@jlu.edu.cn) (W.T. Zheng).

not exactly explained by these two mechanisms have been reported, as porous silicon or nanometric particles [6]. In this letter, we present the first report on the PL features and their temperature dependence of LCMO, which provides another case that cannot be explained by the mechanisms mentioned above. The results indicate that the unconventional features for the electronic structure and their variation with temperature, which arise from the extremely strong coupling among the 3d  $e_g$  conduction electrons, 3d  $t_{2g}$  local spins and lattice [8].

The LCMO polycrystalline samples used in this work were prepared by the standard solid-state reaction method from 99.99% purity oxide and carbonate powders. The X-ray diffraction analysis showed a single-phase perovskite structure of pseudo-cubic symmetry with a lattice constant  $a=0.3865$  nm. The resistivity was measured with the standard four probe method and dc magnetization was measured with superconducting quantum interference device magnetometer (quantum design SQUID). These measurements showed that our polycrystalline samples underwent the ferromagnetic transition at  $T_c=265$  K. The PL spectra of LCMO were recorded in the temperature range 138–293 K using a spectrometer (Jobinyvon company, made in Germany). The samples were excited using  $\text{Ar}^+$  laser with the power of 5 mW and wavelength of  $\lambda=488$  nm.

Fig. 1 displays the PL spectra (1.50–2.50 eV) of the LCMO in the temperature range 138–293 K, for which an excitation laser wavelength of 488 nm was used. The main peak at  $\sim 1.77$  eV, along with the shoulders at  $\sim 1.57$  and  $\sim 1.90$  eV (Fig. 2(a)), respectively, is observed through the whole temperature range. Meanwhile, some features in the range 2.00–2.50 eV can also be observed, which arises perhaps from the interband transitions between the O 2p and Mn 3d bands. These features will not be further discussed. In

the following, we only concentrate on the temperature dependence of PL spectra in the photo-energy range 1.50–2.00 eV, which is shown in Fig. 2(a).

We fit the whole PL spectra by computer software ‘PeakFit’, which is a deconvolution. The computer program PeakFit can accurately detect, separate and quantify hidden peaks that standard instrumentation would miss. As a product of the curve fitting process, PeakFit reports amplitude, area, center and width data for each peak. Overall area is determined by integrating the peak equations in the entire model. PeakFit uses three procedures to automatically place hidden peaks, while each is a strong solution, one method may work better with some data sets than the others. (1) The residuals procedure initially places peaks by finding local maxima in a smoothed data stream. Hidden peaks are then optionally added where peaks in the residuals occur. (2) The second derivative procedure searches for local minima within a smoothed second derivative data stream. These local minima often reveal hidden peaks. (3) The deconvolution procedure uses a Gaussian response function with a Fourier deconvolution/-filtering algorithm. A successfully deconvolved spectrum will consist of ‘sharpened’ peaks of equivalent area.

In this work, the Gaussian line shape is used successfully for fitting the PL peaks, the parameters of the fit, including peak position and integral intensity, are listed in Table 1, Fig. 3 can be plotted from it. Using Gaussian method, the peaks in the PL spectra are deconvolved into three Gaussian peaks, the position of each peak is determined, which is 1.52 eV for  $B_1$ , 1.75 eV for  $B_2$ , and 1.92 eV for  $B_3$  (Fig. 2(b)), respectively, which represent three different types of electronic transitions. The temperature dependence of the intensity for each peak is clearly shown in Fig. 3. In the entire temperature range 138–293 K, the intensity of  $B_1$  increased with increasing temperature, while that of  $B_2$

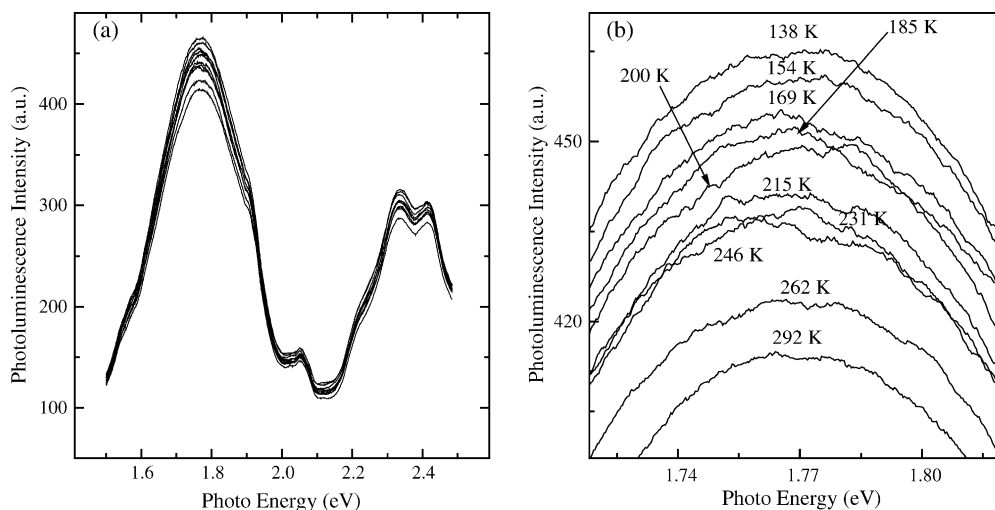


Fig. 1. (a) The visible PL spectra for  $\text{La}_{2/3}\text{Ca}_{1/3}\text{MnO}_3$  under excitation at  $\lambda=488$  nm in the temperature range 138–293 K. (b) The main peak is magnified and the temperature is indicated.

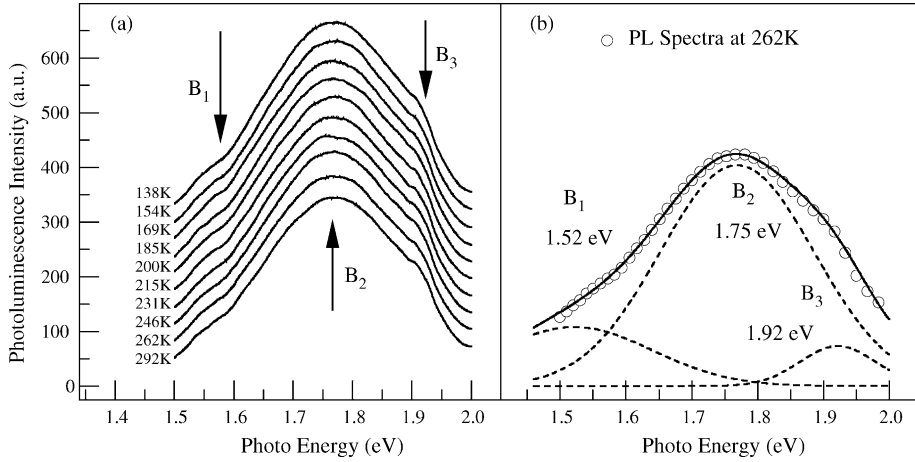


Fig. 2. (a) The PL spectra for  $\text{La}_{2/3}\text{Ca}_{1/3}\text{MnO}_3$  at different temperatures in photo energy range 1.50–2.00 eV and (b) a typical PL spectrum at 262 K, well fitted by three Gaussian curves  $B_1$ ,  $B_2$  and  $B_3$  centered at  $\sim 1.52$ ,  $\sim 1.75$ , and  $\sim 1.92$  eV (open circle: experimental data; solid line: fitting curve).

decreased with increasing temperature. However, the intensity of  $B_3$  is almost temperature-independent.

In order to reveal the mechanisms of PL in LCMO, its related electronic structure should be understood. We note that on studying pulsed laser excitation induced conductance changes in colossal magnetoresistance LCMO on the picosecond time scale, Zhao et al. [8] presented a schematic electronic structure of the  $e_g$  and  $t_{2g}$  levels of  $\text{Mn}^{3+}$  and  $\text{Mn}^{4+}$  ions and the optical transitions in LCMO, as shown in Fig. 4. The upper panel in Fig. 4 shows the energy of Mn  $e_g$  and  $t_{2g}$  levels around the paramagnetic–ferromagnetic transition region for adjacent  $\text{Mn}^{3+}$  and  $\text{Mn}^{4+}$  ions. The spin up  $e_g$  levels in the  $\text{Mn}^{3+}$  ions are split by  $E_{JT}$  due to the J–T effect. In the  $\text{Mn}^{4+}$  the spin up  $e_g$  states are shifted upwards (relative to the unsplit  $\text{Mn}^{3+}$  ion spin up  $e_g$  levels) by  $E_B$  due to the oxygen breathing mode distortion. The spin down  $e_g$  level (not shown in the upper panel) of  $\text{Mn}^{4+}$  is higher by Hund’s coupling energy  $E_J = J_H S_c$  relative to the spin up  $e_g$  level of  $\text{Mn}^{4+}$ , where  $J_H$  is the exchange constant of Hund’s coupling,  $S_c$  is the Mn core spin ( $S_c = 3/2$ ).

Transition A is the dipole active photoionization of the J–T small polarons. The lower panel in Fig. 4 shows the energy levels in the metallic ferromagnetic state at low temperatures. The spin up and spin down  $e_g$  bands are separated by  $E_{JT}$ . The aligned core spins in the  $t_{2g}$  level lie below the spin up  $e_g$  levels by the crystal field energy  $E_C$ . The transition between the spin up  $e_g$  bands and spin down bands, depicted by B, is allowed only by an electric dipole spin flip process. Another possible transition involves electrons from the spin up  $e_g$  level of  $\text{Mn}^{3+}$  to the spin down  $t_{2g}$  level of  $\text{Mn}^{4+}$  with spin flip process. Process C promotes a  $t_{2g}$  core electron of  $\text{Mn}^{3+}$  to the spin up  $e_g$  bands of  $\text{Mn}^{4+}$  by a dipole allowed charge transfer process. The existence of these three transition processes was supported by the temperature dependence of the conductance change deduced from the ultrafast laser conductive and resistive transients Zhao et al. [8] presented. The fact that the visible wide-band emission with a maximum at  $\sim 1.77$  eV can be well fitted by three Gaussian curves  $B_1$ ,  $B_2$  and  $B_3$  centered at  $\sim 1.52$ ,  $\sim 1.75$  and  $\sim 1.92$  eV, respectively, for our samples, indicates that

Table 1  
The fitting parameters of the three Gaussian peaks of  $B_1$ ,  $B_2$  and  $B_3$  at different temperatures

Temperature (K)	Peak position (eV)			Integral intensity (a.u.)		
	$B_1$	$B_2$	$B_3$	$B_1$	$B_2$	$B_3$
138	1.764	1.516	1.923	149.96	13.77	8.56
154	1.769	1.516	1.923	147.49	15.86	6.48
169	1.768	1.528	1.923	145.12	16.38	7.10
185	1.768	1.508	1.923	145.82	16.71	7.17
200	1.772	1.527	1.923	137.35	22.91	6.51
215	1.775	1.520	1.923	135.54	26.69	6.31
230	1.776	1.521	1.923	133.45	28.40	6.10
246	1.779	1.525	1.923	126.09	34.60	6.56
262	1.776	1.517	1.923	99.45	47.91	7.45
292	1.778	1.510	1.923	116.85	47.25	7.78

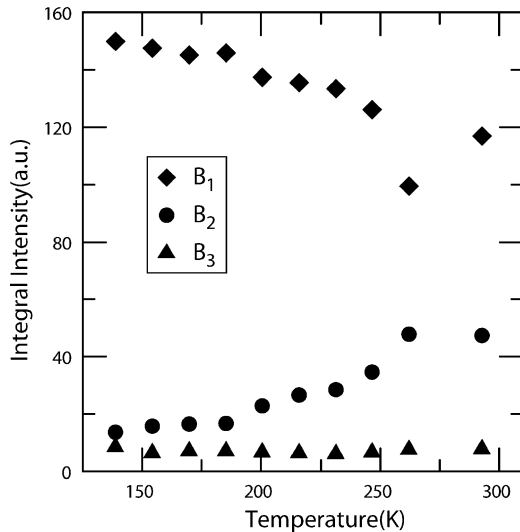


Fig. 3. The temperature dependence of the PL intensities for  $B_1$ ,  $B_2$  and  $B_3$ , which shows that as temperature increases, the PL intensity for  $B_1$  decreases, while that for  $B_2$  increases and  $B_3$  is almost temperature-independent.

this electronic transition model is also supported by our PL results.

The transition energies for the process A, B and C have been evaluated using the existing experimental results [8]. In the optical spectra of LCMO, there is a broad peak in the conductivity function centered around 1.2 eV at room temperature which shifts to lower energies with decreasing temperature [9]. This peak is identified with the charge transfer excitation of an electron from the lower J–T split  $e_g$  level of a  $Mn^{3+}$  ion to the  $e_g$  level of an adjacent  $Mn^{4+}$  ion.

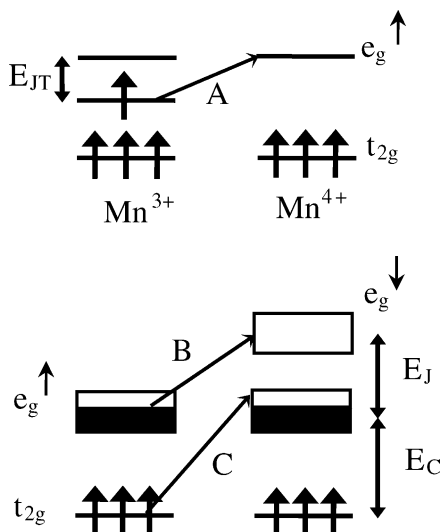


Fig. 4. The schematic electronic structure of the  $e_g$  and  $t_{2g}$  levels of  $Mn^{3+}$  and  $Mn^{4+}$  ions and the optical transitions relevant to the PL peaks.

Because of the significant widths of these energy levels, the excitation can extend into higher photon energy at  $\sim 1.5$  eV [8,9]. This indicates the transition energy of process A can be extended from  $\sim 1.2$  to  $\sim 1.5$  eV. Some experimental results showed that the optical transitions between the spin up  $e_g$  bands and the spin down  $e_g$  bands (process B) were expected to be centered around  $E_J = J_H S_C = 1.7$  eV at low temperature [8,10], whereas the optical process C was the dipole allowed spin conserving  $t_{2g}$  to  $e_g$  charge transfer transition and the  $t_{2g}$  to  $e_g$  crystal field splitting of LCMO was close to 2 eV [8,11]. Based on above experimental results and the peak position of  $B_1$ ,  $B_2$  and  $B_3$  for our samples in Fig. 3, the assignments that  $B_1$ ,  $B_2$  and  $B_3$  correspond to the transition process A, B and C in Fig. 4, respectively, can be made, that is to say,  $B_1$  was identified with the charge transfer excitation of an electron from the lower J–T split  $e_g$  level of a  $Mn^{3+}$  ion to the  $e_g$  level of an adjacent  $Mn^{4+}$  ion,  $B_2$  was assigned to the transition between the spin up and spin down  $e_g$  bands separated by Hund's coupling energy  $E_J$  and  $B_3$  was attributed to the transition, determined by the crystal field energy  $E_C$ , between a  $t_{2g}$  core electron of  $Mn^{3+}$  to the spin up  $e_g$  bands of  $Mn^{4+}$  by a dipole allowed charge transfer process.

The temperature dependence of  $B_1$ ,  $B_2$  and  $B_3$  in PL spectra of LCMO, between which the spectral intensity is exchanged depending on coupling between the 3d  $e_g$  conduction electrons, 3d  $t_{2g}$  local spins and lattice, can be interpreted as follows. Process A corresponds to the photoionization of the J–T splitting of the J–T small polaron. This process would be enhanced with increased J–T splitting of the  $Mn^{3+}$   $e_g$  band as temperature increases, which will increase the overlap of the photon energy with the absorption band. Therefore, the absorption cross section will increase with increasing temperature, which leads to the rise in the intensity of the PL peak at  $\sim 1.52$  eV [8]. The transition B can be realized either between the spin up  $e_g$  bands and spin down  $e_g$  bands or between the spin up  $e_g$  level of  $Mn^{3+}$  and spin down  $t_{2g}$  level of  $Mn^{4+}$  with spin flip process, whereas the process C only involves the transition between a  $t_{2g}$  core electron of  $Mn^{3+}$  and the spin up  $e_g$  bands of  $Mn^{4+}$ . Furthermore, at low temperatures, the J–T effects are not manifest. Hence, the PL intensity for process B is higher than that for either process A or C, as observed in Fig. 3. As temperature increases, the J–T effects become more and more important, which leads to the increase in PL intensity at  $\sim 1.52$  eV. Since, both process A and B involve the electrons at spin up  $e_g$  level, as the hopping transition between J–T split  $e_g$  levels has a higher probability, a corresponding reduction of the transitions to the Hund's split levels  $E_J$  should occur. Qualitatively this is what we observe in the results of Fig. 3. As for the process C, the transition only involves a  $t_{2g}$  core electron of  $Mn^{3+}$  and the spin up  $e_g$  bands of  $Mn^{4+}$ , which is not significantly influenced by temperature. Therefore, the PL intensity at  $\sim 1.92$  eV is almost temperature independent.

In summary, the visible photoluminescence (PL) of

$\text{La}_{2/3}\text{Ca}_{1/3}\text{MnO}_3$  in the temperature range 138–293 K was measured, and its temperature dependence was also presented. It was observed that the main broad peak centered at  $\sim 1.77$  eV along with two shoulders at  $\sim 1.57$  and  $\sim 1.90$  eV existed in the entire temperature range, which can be well fitted by three Gaussian curves  $B_1$ ,  $B_2$  and  $B_3$ . The intensities of the peak  $B_1$  and  $B_2$  varied as temperature increases. In the entire temperature range, the intensity of  $B_1$  increased with increasing temperature, whereas that of  $B_2$  decreased with increasing temperature. The PL mechanisms for  $\text{La}_{2/3}\text{Ca}_{1/3}\text{MnO}_3$  were presented based on the electronic structures formed by the interactions among spin, charge and lattice, in which  $B_1$  was identified with the charge transfer excitation of an electron from the lower Jahn–Teller split  $e_g$  level of a  $\text{Mn}^{3+}$  ion to the  $e_g$  level of an adjacent  $\text{Mn}^{4+}$  ion,  $B_2$  was assigned to the transition between the spin up and spin down  $e_g$  bands separated by Hund's coupling energy  $E_J$  and  $B_3$  was attributed to the transition, determined by the crystal field energy  $E_C$ , between a  $t_{2g}$  core electron of  $\text{Mn}^{3+}$  to the spin up  $e_g$  bands of  $\text{Mn}^{4+}$  by a dipole allowed charge transfer process.

#### Acknowledgements

The support from Chinese Ministry of Education for Excellent Young Teachers in Universities is highly appreciated.

#### References

- [1] S. Jin, T.H. Tiefel, M. McCormack, R.A. Fastnacht, R. Ramesh, L.H. Chen, *Science* 264 (1994) 413.
- [2] P. Schiffer, A.P. Ramirez, W. Bao, S.-W. Cheong, *Phys. Rev. Lett.* 75 (1995) 3336.
- [3] Y. Murakami, J.H. Yoo, D. Shindo, T. Atou, M. Kikuchi, *Nature* 423 (2003) 965.
- [4] C. Zener, *Phys. Rev.* 81 (1951) 440.
- [5] A.J. Millis, P.B. Littlewood, B.I. Shraiman, *Phys. Rev. Lett.* 74 (1995) 5144.
- [6] P.S. Pizani, H.C. Basso, F. Lanciotti Jr, T.M. Boschi, F.M. Pontes, E. Longo, E.R. Leite, *Appl. Phys. Lett.* 81 (2002) 253.
- [7] Y. Okimoto, T. Katsufuji, T. Ishikawa, A. Urushibara, T. Arima, Y. Tokura, *Phys. Rev. Lett.* 75 (1995) 109.
- [8] Y.G. Zhao, J.J. Li, R. Shreekala, H.D. Drew, C.L. Chen, W.L. Cao, C.H. Lee, M. Rajeswari, S.B. Ogale, R. Ramesh, G. Baskaran, T. Venkatesan, *Phys. Rev. Lett.* 81 (1998) 1310.
- [9] S. Kaplan, M. Quijada, H.D. Drew, D.B. Tanner, G.C. Xiong, R. Ramesh, C. Kwon, T. Venkatesan, *Phys. Rev. Lett.* 77 (1996) 2081.
- [10] M. Quijada, J. Cerne, J.R. Simpson, H.D. Drew, K.H. Ahn, A.J. Millis, R. Shreekala, R. Ramesh, M. Rajeswari, T. Venkatesan, *cond-mat/980321*.
- [11] S. Satpathy, Z.S. Popvic, F.R. Vukajlovic, *Phys. Rev. Lett.* 76 (1996) 960.